INSTITUTE OF PHYSICS PUBLISHING EUROPEAN JOURNAL OF PHYSICS

Eur. J. Phys. **28** (2007) 215–230 doi:10.1088/0143-0807/28/2/007

Pattern-forming instabilities: a phenomenological approach through simple examples

Philippe Brunet

Department of Mathematics, University of Bristol, University Walk BS8 1TW Bristol, UK

E-mail: p.brunet@bristol.ac.uk

Received 23 October 2006, in final form 30 November 2006
Published 8 January 2007
Online at stacks.iop.org/EJP/28/215

Abstract

From the streets of clouds to the submarine sand ripples or the striations on the coats of some animals, nature offers many examples of spontaneous patterned structures originating from various instabilities. These patterns can in turn destabilize and show a rich, complex dynamics and possibly end up in disordered behaviours. For over 20 years, these patterns have generated much interest in the physics community, in order to approach fundamental problems such as transition to turbulence or morphogenesis in a more tractable framework. Because the study of such systems needs certain conceptual tools of nonlinear physics and stability analysis, they are generally introduced to students only in post-graduate lectures. We propose here a simplified approach of such phenomena through experimental and numerical examples that can be reproduced with a rather simple set of apparatus: a convection experiment and two gutter-like experiments where a liquid overflows from an overhang, as well as a numerical model consisting of a generic, nonlinear partial differential equation.

(Some figures in this article are in colour only in the electronic version)

1. Introduction

Some physical systems have the striking feature to become unstable by showing a self-organized structure. In the specialized literature, they are generally referred to as 'patterns' or 'cellular structures', where the 'cell' denotes the basic single geometrical shape constituting the pattern. Many books or reviews offer a broad view on these different kinds of patterns and their subsequent dynamics, see e.g. [1–4]. Many examples are found in hydrodynamics, crystal growth, nonlinear optics and even in some chemical reactions. One of the main reasons why these systems attracted a lot of interest in the physics community has been their application to the understanding of collective behaviours in growth or morphogenesis problems.

(a)  (b) 

Figure 1. (a) An example of a structure a snowflake takes during the complex process of its creation. (b) An array of clouds, regularly spaced by the action of convective winds.

Let us take two well-known examples that illustrate the surprising behaviour of pattern formation: (a) the growth of a snowflake and (b) the convection in the atmosphere. In case (a), a complex cycle of condensation, melting and solidification in cold clouds is responsible for the formation of successive thin layers of ice, building from a nucleation site. One may intuitively think that this process, intrinsically isotropic, would give birth to an isotropic round flake. Everyone knows that it is not the case, as illustrated in figure 1(a). Instead, flakes display beautiful patterned structures which break the isotropic initial symmetry, although keeping a lower degree of symmetry in the structure itself. In case (b), something similar happens: convective winds arise from high temperature differences between the ground and the atmosphere or the different levels in the atmosphere. Subsequently, due to buoyancy effects, air should flow vertically and homogeneously from bottom to top. Instead, the flow turns unstable and self-organizes into an array of convective rolls that break the initial translational invariance of the problem. This is often revealed by formations of clouds like those displayed in figure 1(b). The general feature of pattern-forming instabilities is then to exhibit structures having lost symmetries that are present in the underlying initial physical system.

Although these phenomena are broadly observed in nature, they are generally taught late in the curriculum of university student's courses. In recent books of classical mechanics and physics for undergraduate students [5, 6], authors insert more and more often an introductory chapter dedicated to nonlinear dynamics, instabilities and chaos, but they are mostly related to systems with only a temporal dynamics. The extension of concepts of temporal chaos to spatiotemporal disordered dynamics, encompassing pattern-forming instabilities, is generally a further stage in the complexity of mathematical analysis. As a system involving out-of-equilibrium dynamics, its spatiotemporal evolution is strongly influenced by initial conditions. It cannot be figured out by seeking for the local minima of an energy function, contrary to systems in equilibrium thermodynamics for example, and this is one of the reasons that makes the complete analytical resolution of the mathematically difficult problems. However, we propose here that an approach of the physics of patterns can be drawn at a qualitative level, through simple and visual examples. Our aim is not to develop an exhaustive and rigorous theoretical approach of pattern formation, but rather to provide some examples that will give some feeling of different general aspects of this phenomenon. This approach is mainly based on observation and involves examples that allow for an easy display and treatment. The experiments proposed are in the same spirit as those presented in [7], which contains a range of seminal articles on laboratory experiments. In contrast to the examples given in this book, however, we focus on examples where each stage of the formation and dynamics of the pattern

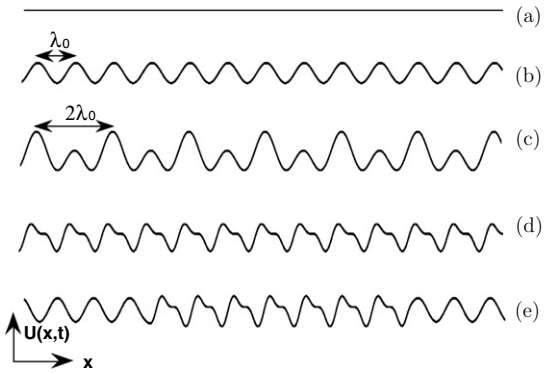

Figure 2. Schematic view of some possible subsequent behaviours on pattern-forming instabilities of moving interfaces, see the text for details.

are clearly identifiable, in terms of clearly observable changes in the symmetries of the system. That is the reason why we deliberately chose to present a certain sub-class of patterns.

The sub-class we would like to present here consists of the so-called interfacial fronts (which has been the subject of a recent review [8]), i.e. the boundary between two immiscible phases, which is subject to an external field (like for example a pressure or a temperature gradient). As for the formation of dendritic structures in snowflakes, such interfacial dynamics can exhibit pattern-forming instabilities. Our choice to show examples of this class of phenomena is motivated by the following: out-of-equilibrium dynamics of interfaces often involve time and length scales suitable for direct observation (contrary to nonlinear dynamics in optics, for instance, that require more sophisticated set-ups).

In all, we present four examples (three experimental and one numerical) of the collective dynamics that can be observed on a destabilizing interface. The experimental systems we chose to present involve time and space scales that allow for easy observations and relatively easy-to-built set-ups. Also, the numerical model is relatively simple to compute and does not require any powerful computing facilities. For each example, a short qualitative description of the phenomenon is given. All of these patterns are spatially extended in only one dimension, which enables the extraction of the complete dynamics in a readable way: if x denotes the only spatial coordinate, the course of time is generally set through a perpendicular axis, which allows to represent the whole dynamics into a bi-dimensional plot called 'spatiotemporal diagram'. To start with, we give a brief introduction of some general aspects of pattern-forming instabilities, as a pedagogical imagery of the phenomenon we will expose afterwards.

2. General phenomenology

As already mentioned, the genesis of patterned structures is due to a break of certain initial symmetries of the system. In a laboratory experiment, this generally appears when one or several control parameters are driven beyond a certain threshold. A primary instability often leads to the appearance of a static periodic network, thus causing the break of the translational invariance. Secondary instabilities may also develop when control parameters are driven beyond secondary thresholds. These new modes, corresponding to new symmetry breaks, can offer a more complex dynamics and can possibly evolve towards disordered states (where spatial and/or temporal dynamics become unpredictable).

To clarify these ideas, figure 2 schematically illustrates examples of generic patterned-forming instabilities in interfacial dynamics. A function $U(x, t)$ represents the interface

deformations [9], where the local maxima can denote the position of cells and where the particular shape of U around these maxima can mimic the shape of cells. An initially plane interface (a) becomes unstable and adopts a cellular, stable periodic solution of wavelength (or spatial period) λ (b), breaking the initial translational symmetry: this is the primary instability. This structure can in turn become unstable through secondary instabilities that break other symmetries. For instance, a doubling of the spatial period can be observed (c), where each initial second cell grows. Even the shape of the cells (i.e. the shape of local maxima) can change: an antisymmetric mode can grow and can cause the break of the left/right (reflexion) symmetry (d). Such a mode can be localized to a few cells (e).

More or less complex collective movements arise from these symmetry breaks. For instance, the spatial period-doubling can be associated with temporal oscillations of cells out-of-phase with nearest neighbours, while modes of reflection-symmetry breaking are associated with drift motions. The combination of these motions can lead to spatiotemporal disorder in a further stage. Thus, there is a close relationship between the local shape of the interface and the wave-like dynamics that develop. This is the reason why we think that these systems are particularly adapted for a pedagogical approach of pattern formation: each step from a basic flat interface towards complex interfacial shape and dynamics can be often identified in terms of broken symmetry. Also, what is remarkable in these systems is that even if the breaking of any symmetry is sometimes not easily observable, effects of the breaking (like the dynamical behaviour) are. This will be more clearly presented in some of the following examples.

3. Pattern formation in a thermoconvective flow

Here, we propose a simple experiment of thermo-capillary convection, from the recent work by J Burguete, D Maza and H Mancini [10]. The principle is to impose a temperature gradient ($\vec{\nabla} T$) to a thin film of liquid bounded by a free surface at its top. The experiment is sketched in figure 3: hot water flowing through metallic pipes imposes the local hot temperature by conduction at the centre bottom of the liquid layer, and a cold water flow imposes the cold temperature along the edges. Since the surface tension γ is temperature dependent, the liquid is subjected to a force at its surface which pulls it from the zones of small γ (high T) towards the zones of large γ (low T). Let us note that the cold water flow is not really required in order to capture the interesting phenomena: as pointed out by the authors, a temperature gradient can take place only due to the action of the central heater which ensures a vertical temperature gradient. The lateral coolers can influence some aspects of the subsequent dynamics of the flow, but not its general feature. The vertical temperature gradient, in the vicinity of the heater, ensures that a hot spot is generated at the free edge on this location. Eventually, a tangential force appears and pulls some liquid from the hot spot towards colder regions, due to surface tension variations at the free surface. The force at the free surface leads to a volume flow by continuity, which in turns brings hot fluid from below and sustains the process. This is the so-called Marangoni effect[1]. As the thickness of the liquid layer is small and thus it makes gravity forces negligible, convection due to surface tension gradients is much larger than buoyant convection in this experiment.

The characteristic lengths of the experiment are the following: the liquid thickness d ranges from 2 to 5 mm, the width of the heater h is around 1 mm, the width of the film l_x is from 4 to 6 mm and the length of the layer l_y is from 200 to 400 mm. The liquid is silicon oil (viscosity 5 mm^2 s^{-1}, surface tension 0.02 N m^{-1}, density 0.91 g cm^{-3}). For very small

[1] This effect is also observed by injecting locally some surfactant: for instance by releasing a drop of soap in water, one generates a flow that pulls the liquid away from the region of the surfactant.

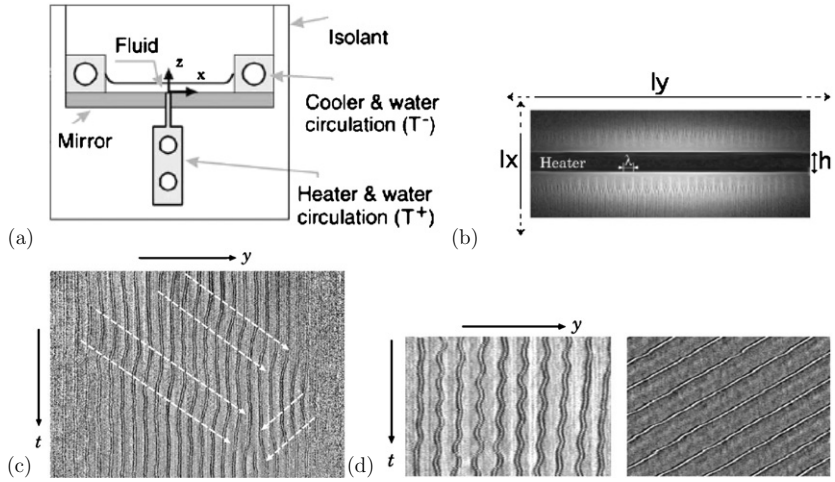

Figure 3. (a) Set-up of thermoconvection experiment in a thin layer of liquid. (b) A view from above of the spatially periodic pattern of rolls. (c) Example of collective dynamics. (d) Dynamical regimes: pure oscillations and drift (illustrations inspired by [10]).

temperature differences ΔT, simple stationary convection is observed. By slightly increasing ΔT, the basic flow becomes unstable and turns to a pattern of convective cells of wavelength $\lambda \simeq 2d$ (the threshold value for the transition depends on the liquid thickness amongst other parameters). This is a general feature of convective flows to self-organize into a pattern; the fluid flows in such a way that heat is transferred more efficiently. A linear stability analysis of the formation of these convective cells is reported in [11]. If the heater element was spatially extended to all the fluid layer, the resulting pattern would be formed by hexagonal cells: then all cells would lie at equal distance to their closest neighbours. Instead, as the heater is a slender element along the y axis, a one-dimensional pattern of rolls appears, oriented perpendicular to the direction of the heater. The translational symmetry of the system along the direction y is broken, which qualitatively reproduces the case of the transition from (a) to (b) in figure 2.

The visualization of such a pattern is achieved by lighting the surface with a laser beam (or by an intense localized source of light), oriented vertically and perpendicularly to the unperturbed liquid surface. The beam is reflected by the mirrors at the bottom of the layer and deflected due to the local variations of the optical index (these variations are due to the variations of T). Figure 3(b) shows an example of such a stationary pattern of convective cells: light lines represent cold areas and dark lines represent hot areas (the central black zone is the heating pipe, where no light is reflected). The addition of small reflective particles, such as aluminium powder or iodine (chemical formula is TiO_2), makes the observation easier. By further increasing ΔT beyond a secondary threshold (between 10 and 20°, smaller for higher d), more complex dynamical regimes appear and break new symmetries of the stationary, spatially periodic state.

Examples of dynamical regimes are provided in figure 3(c), with several examples of the so-called spatiotemporal diagram: the horizontal axis is the spatial direction y, along which convective cells move, and vertical axis is the time t. In such a diagram, a diagonal trajectory like the ones traced in white represents a propagative structure and the speed is directly accessible by evaluating the slope $\Delta y/\Delta t$. To obtain such a diagram, one can extract the light

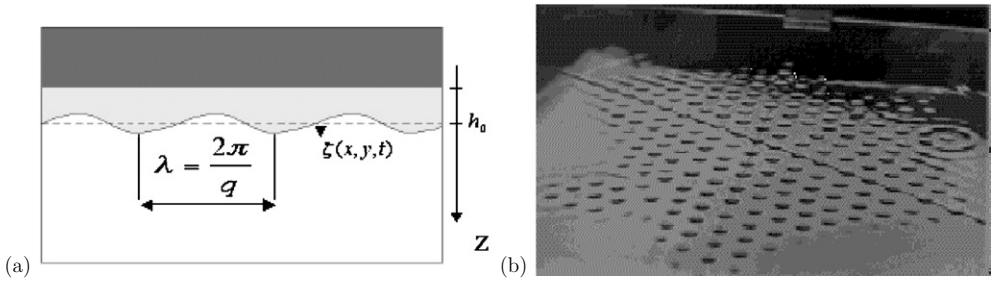

Figure 4. (a) Sketch of the Rayleigh–Taylor instability in one dimension. (b) Network of pending drops, created by the destabilization of a viscous liquid layer hung under a horizontal plate.

levels along a line parallel to y: for example, by using a basic video camera (for instance with CCD elements or a general firewire camera) in combination with the open-source software *Image J*, by Wayne Rasband (available for the main operating systems at the following address: http://rsb.info.nih.gov/ij), and by extracting a line that crosses the pattern (with the copy/paste command). Then, lines for different sequences are piled, to obtain a spatiotemporal diagram. Of course, the extraction/piling procedure can be easily computerized to gain some time: a tutorial to write macros easily is also provided in the web page of *Image J*. Figure 3(d) shows examples of pure, isolated dynamical regimes such as oscillating and drifting cells. Oscillations are rather observed for thin liquid layers ($d < 3.5$ mm), whereas drifting cells appear for thicker layers ($d > 4$ mm). In the last case, the left/right reflexion symmetry of the cells is broken in a way similar to situations (d) and (e) in figure 2, but this break of symmetry is difficult to observe experimentally. Instead, one can measure with a reasonable accuracy the drift velocity of the cells, the group velocity (velocity of domain walls) and the local dilation of drifting cells.

4. Pattern formation of a liquid hung on and flowing from a ceiling

4.1. A two-dimensional network of drops

Liquids flowing from overhangs often lead to unstable behaviours: fountains on public parks, as well as the so-called teapot effect[2] are everyday's life examples. Under its simplest form (i.e. with the lowest possible flow rate), a liquid flowing from an overhang gets structured as a more or less regular network of drops: this is indeed what is observed under a gutter after the rain. Thus, a liquid layer hung under an overhang gets destabilized by developing a pattern of pending drops. A sketch of the phenomenon is given in figure 4(a): it is the *Rayleigh–Taylor instability*. Within the range of liquid thickness and usual liquid viscosity, it is expected that the selection of the spacing between two drops λ (also denoted as wavelength in the following) be governed by two counterbalancing effects: the destabilizing gravity and the stabilizing surface tension. The action of gravity is to amplify any initial tiny perturbation on the layer, whereas surface tension acts as for damping any causes of surface creation between the liquid and the ambient atmosphere. One can understand the causes of this instability by evaluating the increase of energy between an initial flat layer of thickness h_0 and a layer perturbed

[2] This expression denotes the common situation when a liquid is poured from a container to another one. The liquid displeasingly flows along the walls of the source container, if the edges are not sharp enough or if the liquid is not poured with a sufficiently high flow rate.

by a weak-amplitude, periodic deformation ζ (figure 4(a)). Thus, under a one-dimensional overhang of length L, the increase of energy due to gravity is

$$E_{\text{grav}} = -\int_0^L \frac{1}{2}\rho g \zeta^2(x)\,\mathrm{d}x. \tag{1}$$

The additional energy of originating from capillary forces due to surface creation by the deformation is

$$E_{\text{cap}} = \gamma \int_0^L \sqrt{\left(\frac{\mathrm{d}\zeta}{\mathrm{d}x}\right)^2 + 1} - 1\,\mathrm{d}x. \tag{2}$$

The subtraction of the constant term $\int_0^L \mathrm{d}x$ is simply because one evaluates the surface energy from the reference case of a flat interface. By choosing $\zeta = \epsilon \sin\left(\frac{2\pi x}{\lambda}\right)$, with $\epsilon \ll h_0$, the global increase of energy (gravity + capillarity) is

$$\begin{aligned} E_{\text{cap}} + E_{\text{grav}} &= \gamma \int_0^L \sqrt{\epsilon^2(2\pi/\lambda)^2\cos^2(2\pi x/\lambda) + 1} - 1\,\mathrm{d}x - \int_0^L \frac{1}{2}\rho g \epsilon^2 \sin^2(2\pi x/\lambda)\,\mathrm{d}x \\ &= \gamma \int_0^L \epsilon^2(\pi/\lambda)^2(\cos(4\pi x/\lambda) + 1)\,\mathrm{d}x - \frac{1}{4}\rho g \epsilon^2 \int_0^L (1 - \cos(4\pi x/\lambda))\,\mathrm{d}x \\ &= \epsilon^2 L\left(\pi^2 \gamma \frac{1}{\lambda^2} - \frac{1}{4}\rho g\right). \end{aligned} \tag{3}$$

The approximation of small deformations ($\epsilon \ll h_0$) enables to simplify the second line. The integral of the gravity term is simply $\frac{1}{2}\rho g L \epsilon^2$, independent of the value of λ. However, the surface energy term depends on λ as $\sim\lambda^{-2}$, which causes the damping of short-wavelength perturbations. Indeed, the surface tension reflects the natural tendency for liquids to adapt their shape in order to minimize the surface of their interface with the surrounding gas or another immiscible liquid. In order that the deformation leads to a decrease of the total energy, the following condition is found:

$$\lambda > 2\pi\sqrt{\frac{\gamma}{\rho g}}. \tag{4}$$

For our experiments, silicon oil (of chemical name poly-dimethylsiloxane) is used, as its low surface tension ($\gamma = 0.0205$ N m^{-1}) enables the perfect wetting of the overhang. These oils exist for a very large range of viscosities, from $\nu = 0.5$ mm^2 s^{-1} to more than 10^6 mm^2 s^{-1} (appearing almost like a solid then), depending on the reticulation rate of the polymer[3]. The density of silicon oil is between $\rho = 0.92$ g cm^{-3} and $\rho = 0.97$ g cm^{-3} (increasing with the reticulation rate, as does the viscosity). The critical wavelength λ_c is then evaluated around 0.9 cm. Any perturbation of wavelength larger than λ_c will be amplified.

Practically, it is observed that a well-defined wavelength λ_{RT} is selected, and it is possible to show that this wavelength is associated with the spatial mode with the largest growth rate (then the one which gets amplified the fastest)[4]. For the silicon oil, the wavelength associated with this maximal growth rate is equal to 1.30 cm. The exact value is given by the equation $\lambda_{RT} = 2\pi\sqrt{2}\sqrt{\gamma/\rho g}$. Such an analysis goes beyond the scope of this paper, but the reader can find it in details in [12, 13]. Let us keep in mind here that a wavelength is preferentially selected during the first stages of the instability and that this wavelength matches the condition given by the basic calculus that has led to equation (4). Such a selection is evidenced by the

[3] Cooking oils do not match the required conditions of this experiment, as their viscosity is generally too small.

[4] The growth rate $\sigma(\lambda)$ represents the inverse of a characteristic time in the linear regime (growth of initial small perturbations). Any small sinusoidal perturbation of wavelength λ grows like $\sim\exp(\sigma t)$, where t standing for time.

picture of figure 4(b), representing a two-dimensional pattern of pending drops, developing when a glass plate coated by a thin layer of viscous liquid is suddenly put upside down.

The suitable experimental conditions for an easy observation of the development of the pattern (i.e. reasonable time scales) are the following [12]: one coats the plate with a certain amount of oil (viscosity around 1000 $mm^2\ s^{-1}$ or larger), in order to obtain a uniform thickness of a few tenth of millimetres (the complete spreading can take almost two days for very viscous oils). During the spreading procedure, it is particularly important to avoid that the boundary of the spreading liquid 'pancake' gets pinned to the edge of the plate. This boundary is usually referred to as the contact line, as it is the physical line where liquid, solid and vapour phases meet. In a second step, the plate is put upside down, and then an unstable situation due to gravity is created. The growth of pending drops then starts, the characteristic time of which depends on the viscosity and on the thickness: the higher the ν and the smaller the thickness are, the slower the drops grow. For typical values of viscosities and thicknesses already advised above, the time of growth is of the order of several hundreds of seconds. Hence, the formation of drops can be easily observed. The deformations of the layer can be acquired by a camera from above, lighting from below. As the oil is transparent, the observation of these deformations can be enhanced by placing a transparent grid (in practice, a graphic paper photocopied on a slide), the deformations of which are very sensitive to the slope of the liquid layer. An alternative method is to add some dye in the oil, since the local amount of light then depends on the local thickness.

Without any geometrical constraint, the drops spontaneously self-organize in a hexagonal network (figure 4(b)), thus matching the condition of a well-defined selected wavelength leading to an equal spacing between each pair of drops. Indeed, the hexagonal network ensures that each drop can see all its nearest neighbours at equal distance. This would not be the case for a square network, for instance, as some of the neighbours would be distant from λ and other neighbours would be distant from $\sqrt{2}\lambda$. It is however possible to counteract to this natural tendency, by introducing some geometrical constraints. For example, by sticking two perpendicular thin wires, of a thickness smaller than that of the unperturbed liquid, a square network can be locally forced to develop in the vicinity of the wires, competing with the natural tendency of the instability. Also, by perturbing the layer with small disc-shaped pins forming a pattern on the glass plate (before coating it), with spacing slightly different from the natural selected wavelength, one would force another wavelength to appear. Under more general considerations, such an out-of-equilibrium system chooses a state which is strongly dependent on initial conditions or imposed perturbations; on the other hand, the regular hexagonal structure of wavelength λ_{RT} is obtained from an unperturbed initial layer. Playing with the balance of these two tendencies is certainly one of the most instructive aspect of this experiment.

4.2. A one-dimensional pattern of liquid columns

The previously described experiment is a first view of a pattern structure of drops arising from a competition between gravity and surface tension forces. We now propose to extend this situation to the case where drops are replaced by liquid jets (also denoted as columns) if the overhang is continuously fed with liquid at a high enough flow rate Q. Figures 5(a) and (b) show a pattern of liquid columns forming under a hollow cylinder (a) and a circular dish (b). Around the latter, a scheme of the hydraulic circuit is represented. The continuous supply of liquid is ensured by a reservoir placed at around 2 m above the overhang. The reservoir itself is supplied with liquid by a pump. It is also possible to feed the overhang directly from the pump, but in this case it is important not to use a pump with large pulsation or to damp

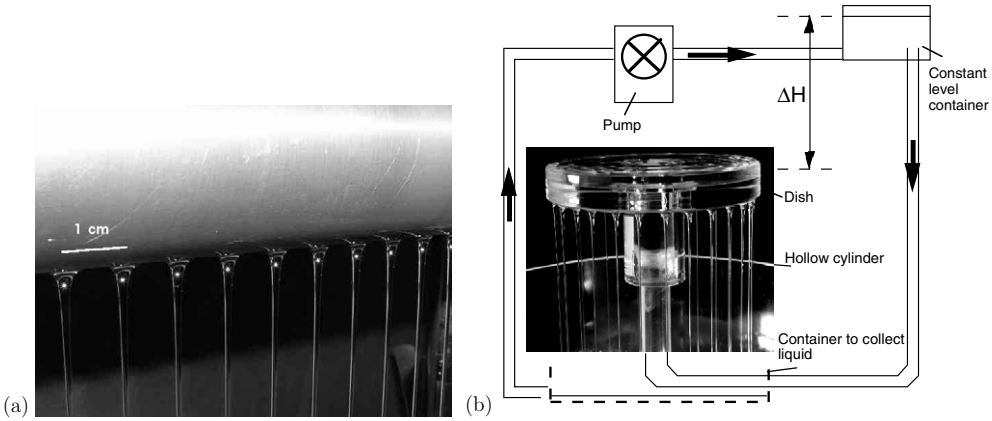

Figure 5. Network of liquid columns hung under an overhang constantly fed with liquid. (a) Under a horizontal hollow cylinder, the overflowing liquid creates a one-dimensional array of liquid columns. (b) A same network of columns is formed when the liquid overflows from a circular dish, but without any edge.

the pulsation: for instance by pushing the liquid through a hollow cylinder that is connected to the centre of the dish, the flow is not pulsed when the liquid is supplied at the dish. The range of flow rates to form the pattern of columns is between 0.05 $cm^2\ s^{-1}$ and 0.5 $cm^2\ s^{-1}$ per centimetre of overhang. Then for a dish of diameter 10 cm, a perimeter of overhang of around 30 cm, the range of flow rate is between 1.5 $cm^3\ s^{-1}$ and 15 $cm^3\ s^{-1}$. This is the natural control parameter, and a variation of its value directly leads to significant changes in the dynamics of the pattern.

Once again, a suitable liquid for the experiment is silicon oil with viscosities from 10 $mm^2\ s^{-1}$ and beyond, although the richest dynamics are observed for viscosities around and above 100 $mm^2\ s^{-1}$. Although the choice of silicon oil is based on the large range of viscosities available, cooking oil (with viscosities between 50 and 70 $mm^2\ s^{-1}$) offers a practical cheaper alternative. It is important to choose a relatively viscous liquid that also has a low surface tension in order to perfectly wet the overhangs (for instance, glycerine does not wet well usual solids and then is not suitable here). However, a limitation for the use of high viscosities is the power of the pump itself: the more viscous, the more difficult to make the liquid flow through the pipes.

Hence, a continuous supply of liquid allows for the liquid to form this pattern of columns, whereas without this supply or at a too small flow rate, columns would pinch off into dripping sites. It turns out that each of these columns can move along the liquid layer that coats a circular area (for the dish) or a line area (for the cylinder) below the overhang. Not only columns move along this circle or line, but also their motion is strongly related to the motion of their nearest neighbours. Thus in a way similar to the thermoconvection experiment, the pattern of columns displays collective dynamics. The motions of columns are related to local symmetry breaks, which is clearly visible by carefully observing the shape of the interface on arches between two columns (figure 6(a)): the arch between two static columns tends to remain symmetrical (top), whereas it opts for an asymmetrical shape between two drifting columns (bottom). The break of the left/right reflexion symmetry reminds the one illustrated in figure 2 (cases (d) and (e)), and it is a generic feature of this class of patterns [1, 9]. A drift motion of columns is associated with the symmetry break as well as with a local dilation of the pattern. Although, the spacing between static columns (wavelength) is quite close to the

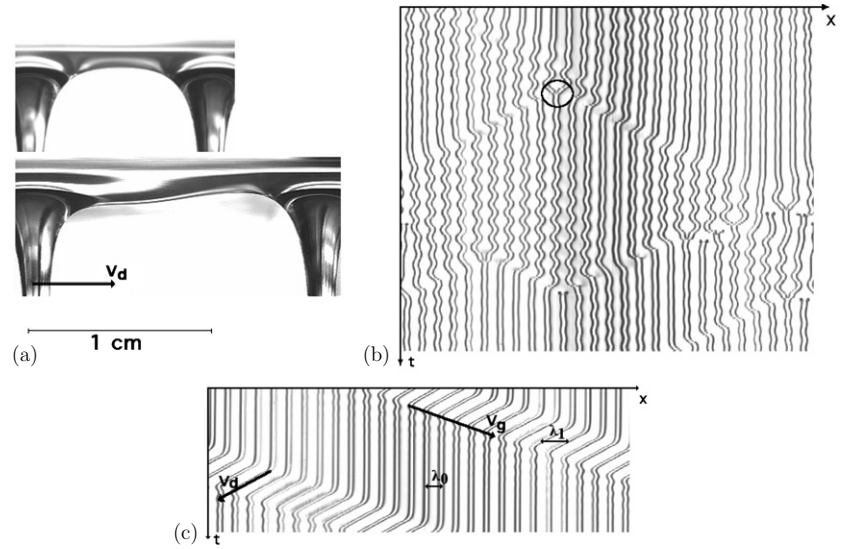

Figure 6. (a) Illustration of the left/right symmetry break on the arch of fluid between two drifting columns. Up: static columns. Down: drifting columns. (b) Example of a spatiotemporal diagram in a chaotic regime: the position of the columns along x (horizontal axis) versus time t (vertical axis). The merging of two columns (surrounded by a black circle) leads to the generation of propagative domains. (c) The spatiotemporal diagram of a single propagative domain and some measurable quantities.

spacing between pendant drops (between 1 and 1.2 cm for silicon oil), the distance between moving columns ranges from 1.6 to 2.2 cm. Thus, the motion of columns and the associated break of symmetries can be initiated by creating a local dilation: for instance, by driving a column with a thin sharp object (a needle) soaked through the top of it and by forcing it to merge to neighbouring columns. Other columns will move towards the gap created and will initiate a local domain of drifting columns. Thus with some accuracy, the experimentalist can control the number of columns, their relative speed and spacing in an easy way. By suppressing enough columns, one can even access a state where all the columns drift at the same speed. One retrieves a property of out-of-equilibrium systems: the final reached state strongly depends on initial conditions, and in the pattern of columns these initial conditions are related to the number of columns, their position and speed. Other dynamical states, for instance where columns oscillate out-of-phase with their nearest neighbours, can be obtained by 'playing' with the position and speed of columns [14]. Under some conditions (a viscosity around 100 $mm^2\ s^{-1}$ and a high enough flow rate), a chaotic state is obtained, where the columns move erratically. In such a situation, spontaneous splitting or merging of neighbour columns are observed.

The patterns of columns formed below both the hollow cylinder and the circular dish are essentially of same nature, but the dish offers the advantage to get rid of edge effects that would bring unwanted perturbations otherwise. Furthermore, propagative domains can move along the dish without encountering the boundary. Whatever the overhang shape, it is of first importance to ensure it is perfectly horizontal: in practice, the set-up should be put on a tuneable three-feet table.

The use of a transparent medium for the overhang allows for accessing the detailed dynamics of columns. Let us now consider the case of the circular dish. By taking pictures of the dish from above, it is possible to access the position of each column versus time,

provided that the dish is made of a transparent medium like plexiglass. The dish has to be homogeneously lighted, and then each column appears as a dark outline. With this set-up, it is possible to build a spatiotemporal diagram, in the same way as in the thermoconvection experiment, by extracting grey levels along a circle intercepting the centres of columns and by 'unfolding' this circle to a line. Such a macro and its open source are available for free downloading with the *Image J* software: it is called 'Oval extraction'. A one-dimensional array of grey or colour levels (from 0 to 255 for a 8 bits picture) is obtained, which can be traced as a horizontal line. By piling these resulting lines one below another, one reconstructs diagrams such as shown in figures 6(b) and (c), where the axis x stands for the spatial coordinate (the left and right boundaries are then connected, as the circular dish provides periodic boundary conditions) and vertical axis t represents the course of time.

Let us have a look on the general dynamics of this pattern. Figure 6(b) is a disordered regime: one clearly sees an erratic motion of columns. However, this disordered regime contains blocks of ordered dynamical regimes, like patches of oscillating columns with spatial period-doubling (similar to the ones observed in thermoconvection, figure 3(d), and described in case (c) of figure 2). In disordered regimes, one also notices the occurrence of structural 'defects', i.e. the sudden splitting or merging of two columns. One of these defects is pointed out by a circle, and one can remark that two propagative structures are launched at its trail. Figure 6(c) represents one of these propagative domains, inside which columns are drifting. It lies in a situation where it exists isolated, and then it can propagate endlessly, as long as the liquid is supplied. These diagrams enable a quantitative study of the propagative domains, by providing a direct measure of the velocity drift of the columns (V_d), the velocity of the domain walls ('group' velocity V_g), and the wavelengths inside (λ_1) and outside (λ_0) a domain. Most of these quantities depend on the flow rate [14], and the velocities increase with the spacing between columns. At a more qualitative stage, it is instructive to build a diagram of stability of the different regimes (static columns, oscillations, propagative domains, global drift, chaos) varying both the flow rate and the mean wavelength λ_m (the latter quantity is varied through the number of columns). Hence, one obtains a two-dimensional mapping that includes the sub-domains of parameters in flow rate Q and λ_m where these regimes are stable [14].

5. A generic simple model: the Kuramoto–Sxivashinsky equation

Here, we propose an example of partial differential nonlinear equation that reproduces, at least qualitatively, some of the features of the experiments presented above. Thereafter we give a commented code that solves this equation numerically and examples of the dynamics that it exhibits. We use the so-called stabilized Kuramoto–Sivashinsky equation (SKS), proposed here in its spatially one-dimensional version. It is a simple generic model that allows for spatially periodic solutions which can destabilize in various different ways, depending on the range of control parameters. It is denoted as 'simple', as it contains the lowest possible orders of spatial derivatives and their nonlinear combinations, and still describes the behaviour of a pattern-forming unstable interfacial front [15]. Hence, the destabilization scenarios are very similar to those of figure 2. Like in this basic scheme, the front is represented by a function $u(x, t)$: each cell of the pattern is represented by a local maximum of the function u. Note that all terms of the equation respect the initial symmetries of the system, i.e. the spatial translation invariance $x \to u + cte$ and the left/right symmetry invariance (if $u(x, t)$ is a solution, so is $u(-x, t)$). The SKS equation is written as

$$\frac{\partial u}{\partial t} = -\alpha u + \beta \left(\frac{\partial u}{\partial x}\right)^2 - \gamma \frac{\partial^2 u}{\partial x^2} - \delta \frac{\partial^4 u}{\partial x^4}. \tag{5}$$

A suitable rescaling enables to fix parameters β, γ and δ equal to one, without loss of generality. The aim is here to study the stability and the possible destabilization scenarios of spatially periodic solutions, those representing basic states of patterned structures. A typical 'numerical experiment' consists of calculating the spatiotemporal evolution of an initial interfacial patterned solution $u_0 = u(x, t_0)$, which in practice can be chosen like a combination of sine functions. The parameters to be fixed are then the initial main wave number k, the damping coefficient α, and the different amplitudes (A_i) and phase shifts (ϕ_i) of the possible other terms in the sine combination of the initial condition. The initial function then takes the general form $u_0(x) = A_0 \sin(kx) + A_1 \sin(n_1 kx + \phi_1) + \cdots$. n_i are strictly positive integers. The choice for n_i, A_i and ϕ_i directly influences the final solution. Otherwise, it is possible to change at will the number of cells, from a spatially constrained system (with 2 or 3 cells) to a more extended system (10–20 cells).

Description of the code provided in the appendix

The solution of equation (5) needs a little computational power, which makes it feasible by personal computers. The code given in appendix is written in Matlab 7.0 (and also works in previous 6.x versions). We use a pseudo-spectral method: the nth derivative is evaluated in Fourier space, by multiplying each kth term of the Fourier decomposition of u by $(ik)^n$. This method is very fast, simple, and broadly used for periodic or pseudo-periodic solutions of PDEs. The code plots the spatiotemporal evolution of the patterned interface and its Fourier transform until the final time is reached. To mimic the spatiotemporal diagrams obtained in experiments, the function f is plotted with a shift proportional to time, along the vertical axis.

Let us comment the code step by step: the value of $k = 2\pi/\lambda$ is first fixed (with λ being the wavelength of the initial solution). Typical values for k range from 0.4 to 0.9, where the most interesting phenomena (or at least the most comparable to experiments) occur. Below $k = 0.4$, the cells are too dilated and quickly split, which leads to local nucleation of new cells and eventually increases k. Above $k = 0.9$, cells are too compressed and merge by pair of two neighbours, which leads to a decrease of k. The variable *Nx* holds for the number of points for the calculation along the spatial coordinate x. *Ncell* denotes the initial number of cells (the typical values being 3–30 cells), and suitable values for *Nx* range from 10 to 16 times *Ncell*, and one has to try if possible to have it equal to a power of two (which makes the fast Fourier transform faster). If *Nx* is too small, the profile of the interface is too rough, whereas if it is too large a numerical artefact makes the calculation diverge (unless one also decreases the value of the time step, which drastically increases the required computational time). The next line of the code determines the x coordinates on which the values of v are evaluated. The two next lines create *kxvect*, an array including the different values of wave number, corresponding to the Fourier coefficients of u to be calculated. This array will be used to determine the successive derivatives in Fourier space. Then, the parameters of the equation are fixed. The next lines set various initial conditions: the most natural one contains only one sine term ($A_i = 0$ if $i \geqslant 1$), but the choice of alternative initial conditions, like the one proposed as (C2), appears to be necessary to allow for the convergence towards certain states. For instance, starting with asymmetric cells makes it possible to reach drifting regimes with cells of broken left–right symmetry. Then, depending on which state one aims to study, one chooses an initial condition and comments out the others possible initial conditions. Then, the code defines the time step *dt*, which is necessarily small to avoid convergence problems. The time index *ind* is initialized, as well as the vertical shift of plotted interfaces *incplot* and the index of the number of plots *plotcont*. The calculation loop: the Fourier transform *uf* is evaluated by the Matlab function *fft*. The power spectrum *pw* is in turn evaluated. Successive

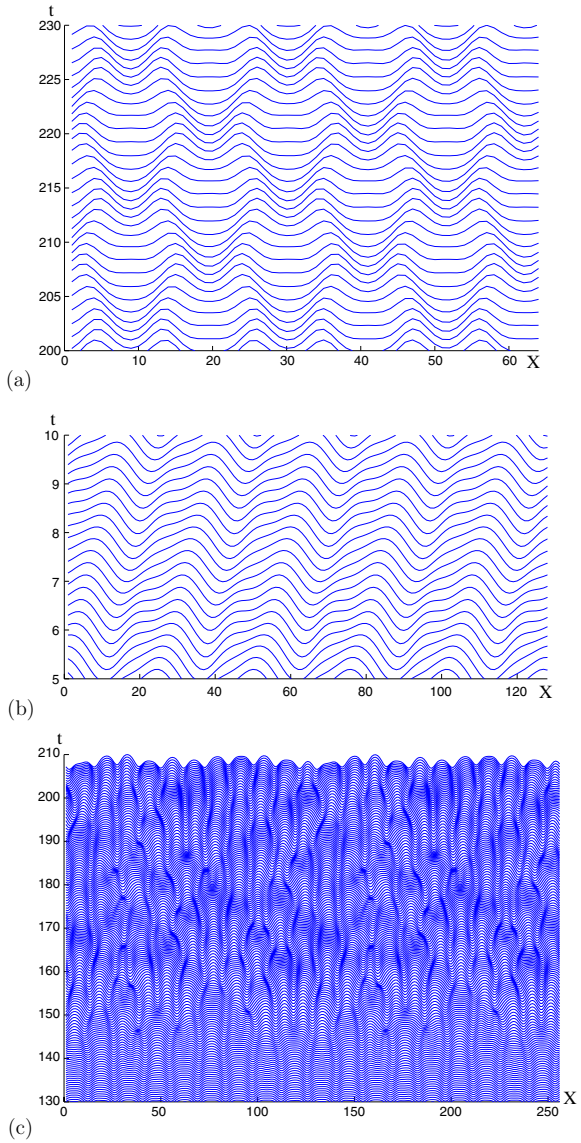

Figure 7. Examples of dynamical behaviours in the cellular solutions of the SKS equation.

derivatives are calculated in Fourier space by a vectorial multiplication of the array of wave numbers *xvec*, times the imaginary i: this is the principle of the pseudo-spectral method. To go back in real space, an inverse Fourier transform is done, also with a function provided in Matlab *ifft*. Each time a time step is a multiple of the variable *tracestep*, the function v and the power spectrum of its Fourier transform pw are plotted. The axis positions are defined in order to include the evolutions of the profile. After the loop, the new value of u is evaluated, with an explicit determination of its time derivative given by equation (5). Then, one returns to the beginning of the loop, to calculate the new Fourier transforms.

Figures 7(a)–(c) illustrate examples of dynamical evolutions of the interface function $u(x,t)$: (a) cells oscillate out-of-phase with respect to their nearest neighbours, (b) reflexion

symmetry-broken cells drift at constant speed and (c) an initially static state which turns disordered, with occurrences of defects (birth of one column or merging of two columns in one). The values of parameters corresponding to these situations are given as examples:

- Oscillating state: $\alpha = 0.10$, $k = 0.64$, initial condition: sinus + random perturbations (C1).
- Drifting state: $\alpha = 0.15$, $k = 0.47$, initial condition: sum of two sinus, of wave number ratio $1/2$ and with a phase shift creating reflexion symmetry-broken cells (C2).
- Chaotic state: $\alpha = 0.08$, $k = 0.53$, initial condition: sinus + random perturbation (C1).

The tracking of the shape of the interface allows to better encompass the importance of the second-order harmonic in the motion of cells (drift or oscillations). In this sense, the plot of the Fourier transform (in fact, of the power spectrum) illustrates the growth of higher order modes during various destabilization scenarios and final states. A typical study is to determine a stability diagram, varying for instance k and α. If the choice of two values (k, α) leads to the break of the pattern of the initial solution, one can try to operate with antisymmetric cells by trying the alternative initial conditions (C2).

6. Conclusion

We have given an introductory phenomenological view of pattern-forming interfaces, through some experimental and numerical examples. More generally, we have shown how the break of some local or global symmetries can lead to dynamical behaviour.

We have deliberately chosen to propose systems that are spatially extended in only one dimension, for the sake of phenomenological clarity and as the experiments are easy to carry out. The three proposed experimental systems possess length and time scales which enable easy observation and analysis.

Our hope is that these examples will encourage the development of analogous experiments, as an introductory part of nonlinear dynamics and symmetry-breaking phenomena. There exist many other examples of pattern-forming systems in the literature [1, 2, 4, 7], such as a liquid layer submitted to vertical vibrations (a set of waves produced by the Faraday parametric instability), a viscous liquid layer flows down an incline (formation of a fingering pattern) or a layer of sand put into a shear flow (ripples formation). Such experiments, which do not require sophisticated equipments, can constitute original subjects for practical works.

Acknowledgments

M M Jérôme Hoepffner and Luca Brandt are kindly acknowledged from their help in the numerical resolution of the SKS equation. Jacco Snoeijer is gratefully acknowledged for a critical reading of the manuscript. The figures of the thermoconvective experiments have been reproduced from [10], with courtesy of the authors and the editor of *Physica* D.

Appendix. Matlab code of the numerical resolution of the SKS equation

```
clear
figure(1), clf
figure(2), clf
k=0.64; lambda=2*pi/k;
```

```
% Wavenumber and wavelength of the initial cellular solution
Ncell=10;
% Number of cells
Nx=128;
% Number of points of the interface on which u is evaluated (10 to
16 times Ncell)
x=linspace(0, Ncell*lambda, Nx+1);
% Defines the points where $u$ is evaluated
kxvec=0 : 2*pi/x(end) : 2*pi/x(end)*Nx/2;
% Creation of the array of the wavenumber values
k=[kxvec(1 : end-1) -fliplr(kxvec(2 : end))];
% The negative wave-numbers (mirrored from the positive values) are
concatenated
alpha=0.1;
% Physical parameters of the equation
beta=1; gamma=1; delta=1;
u(1 : Nx) = sin(k*x(1 : Nx)+rand(1, Nx)/10);
% Initial condition (C1)
%u(1, Nx) = sin(k*x(1 : Nx))+0.5*sin(2*k*x(1 : Nx)+0.5);
% Alternative initial condition (C2)
dt=0.001;  % Time-step
ind=0; incplot=0.5; plotcont=0;
% Shift on the vertical axis at each new time step
tracestep=1000;
while ind<10000000
uf=fft(u)/Nx;
% Calculation of the Fourier transform and the successive derivatives
pw=uf.*conj(uf);
ufx=i*k. *uf;
ufxx=-k. ^2. *uf;
ufxxxx=k. ^4. *uf;
u=real(ifft(uf)*Nx);
% Back to the physical space
ux=real(ifft(ufx)*Nx);
uxx=real(ifft(ufxx)*Nx);
uxxxx=real(ifft(ufxxxx)*Nx);
if mod(ind, tracestep)==0
% The function is plotted every tracestep time steps
  plotcont=plotcont+1;
```

```
    figure(1)
    axis ([0 Nx incplot*plotcont-20 incplot*plotcont+10])
    hold on
    plot(u+incplot*plotcont)
    % Plot of the calculated function, shifted on the vertical axis
    figure(2)
    plot(k, real(pw))
    % Plot of the Fourier transform
    axis ([-max(k) max(k) 0 0.5])
end
U=-(alpha*u+beta*ux.^2+gamma*uxx+delta*uxxxx);
% Evaluation of u at the next time step
u=dt*U+u;
ind=ind+1;
end
```

References

[1] Cross M C and Hohenberg P C 1993 Pattern formation outside of equilibrium *Rev. Mod. Phys.* **65** 851
[2] Rabinovich M I, Ezersky A B and Weidman P D 1998 *The Dynamics of Patterns* (Singapore: World Scientific Publishing)
[3] Manneville P 1990 *Dissipative Structures and Weak Turbulence* (New York: Academic)
[4] Birikh R V, Briskman V A and Velarde M G 2003 *Liquid Interfacial Systems: Oscillations and Instability* (New York: Dekker)
[5] Taylor John R 2005 *Classical Mechanics* (Sausalito, CA: University Science Book)
[6] McCauley J L 1997 *Classical Mechanics: Transformations, Flows, Integrable and Chaotic Dynamics* (Cambridge: Cambridge University Press)
[7] Lam L (ed) 1998 *Nonlinear Physics for Beginners: Chaos, Pattern Formation, Solitons, Cellular Automata and Complex Systems* (Singapore: World Scientific Publishing)
[8] Saarloos W van 2003 Front propagation into unstable states *Phys. Rep.* **386** 29–222
[9] Goldstein R E, Gunaratne G H, Gil L and Coullet P 1991 Hydrodynamics and interfacial patterns with broken space-time symmetry *Phys. Rev.* A **43** 6700
[10] Burguete J, Maza D and Mancini H L 2003 One-dimensional dynamics in locally heated liquid layers *Physica* D **174** 56
[11] Davis S H 1987 Thermoconvective instabilities *Ann. Rev. Fluid Mech.* **19** 403–35
[12] Fermigier M, Limat L, Wesfreid J E, Boudinet P and Quillet C 1992 Two-dimensional patterns in Rayleigh–Taylor instability of a thin layer *J. Fluid Mech.* **236** 349
[13] Chandrasekhar S 1961 *Hydrodynamic and Hydromagnetic Stability* (Oxford: Clarendon) (reprinted by Dover (1981))
[14] Brunet P and Limat L 2004 Defects and spatiotemporal chaos in a pattern of falling liquid columns *Phys. Rev.* E **70** 046207
[15] Misbah C and Valance A 1994 Secondary instabilities in the stabilized Kuramoto–Sivashinsky equation *Phys. Rev.* E **49** 166